INSTITUTE OF PHYSICS PUBLISHING PHYSICS IN MEDICINE AND BIOLOGY

Phys. Med. Biol. **48** (2003) 2405–2418 PII: S0031-9155(03)58338-5

Can the cerebral metabolic rate of oxygen be estimated with near-infrared spectroscopy?

D A Boas[1], G Strangman[1,2], J P Culver[1], R D Hoge[1], G Jasdzewski[1], R A Poldrack[1,3], B R Rosen[1] and J B Mandeville[1]

[1] Athinoula A Martinos Center for Biomedical Imaging, Massachusetts General Hospital, Harvard Medical School, Charlestown, MA 02129, USA
[2] Neural Systems Group, Massachusetts General Hospital, Harvard Medical School, Charlestown, MA 02129, USA
[3] Department of Cognitive Psychology, University of California, Los Angeles, CA 90095, USA

Received 13 January 2003, in final form 17 June 2003
Published 22 July 2003
Online at stacks.iop.org/PMB/48/2405

Abstract

We have measured the changes in oxy-haemoglobin and deoxy-haemoglobin in the adult human brain during a brief finger tapping exercise using near-infrared spectroscopy (NIRS). The cerebral metabolic rate of oxygen ($CMRO_2$) can be estimated from these NIRS data provided certain model assumptions. The change in $CMRO_2$ is related to changes in the total haemoglobin concentration, deoxy-haemoglobin concentration and blood flow. As NIRS does not provide a measure of dynamic changes in blood flow during brain activation, we relied on a Windkessel model that relates dynamic blood volume and flow changes, which has been used previously for estimating $CMRO_2$ from functional magnetic resonance imaging (fMRI) data. Because of the partial volume effect we are unable to quantify the absolute changes in the local brain haemoglobin concentrations with NIRS and thus are unable to obtain an estimate of the absolute $CMRO_2$ change. An absolute estimate is also confounded by uncertainty in the flow–volume relationship. However, the ratio of the flow change to the $CMRO_2$ change is relatively insensitive to these uncertainties. For the finger tapping task, we estimate a most probable flow–consumption ratio ranging from 1.5 to 3 in agreement with previous findings presented in the literature, although we cannot exclude the possibility that there is no $CMRO_2$ change. The large range in the ratio arises from the large number of model parameters that must be estimated from the data. A more precise estimate of the flow–consumption ratio will require better estimates of the model parameters or flow information, as can be provided by combining NIRS with fMRI.

1. Introduction

A robust and reliable measure of the cerebral metabolic rate of oxygen ($CMRO_2$) would provide an important tool for exploring the neural–metabolic–haemodynamic relationship

during cerebral activation under normal and patho-physiological conditions. Positron emission tomography (PET) provides the most direct measure of $CMRO_2$ by imaging the accumulation of ^{15}O labelled radiotracers in the brain (Mintun *et al* 1984). PET, while providing quantitatively accurate images of $CMRO_2$, is restricted in terms of the number of repeated measurements in an individual and the temporal resolution (generally >30 s) (Budinger 1998, Ross *et al* 1997), which limits its applicability and precludes study of transient changes in oxygenation associated with neuronal activation. Advances in functional magnetic resonance imaging (fMRI) are being made to obtain an indirect measure of $CMRO_2$ changes ($\Delta CMRO_2$) from alterations of blood oxygenation and blood flow. This is achieved by simultaneously measuring changes in cerebral blood flow (ΔCBF) and the blood oxygen level dependent signal (BOLD) (Davis *et al* 1998, Hoge *et al* 1999b, Kim 1995, Schwarzbauer and Heinke 1999). The fMRI estimate of $\Delta CMRO_2$ potentially has good spatial and temporal resolution, but is indirect, as it requires assumptions about the relationship between ΔCBF and changes in cerebral blood volume (ΔCBV), and requires a calibration of the scaling factor between the BOLD signal and the deoxy-haemoglobin concentration, usually using a hypercapnic episode (Davis *et al* 1998). While ΔCBV is difficult to measure in humans during cerebral activation with fMRI, it is being done in animals with MION contrast agent (Mandeville *et al* 1998, 1999a), removing one of the assumptions in the estimate of $\Delta CMRO_2$. Unfortunately, suitable iron oxide contrast agents are not approved for use in human subjects, and there is no way to simultaneously obtain information about flow, oxygenation and blood volume changes with fMRI.

Near-infrared spectroscopy (NIRS) provides an approach to estimating $\Delta CMRO_2$ that is similar to the fMRI approach; that is, estimating $\Delta CMRO_2$ indirectly from haemodynamic parameters. NIRS has an advantage over fMRI in that it provides a direct measure of oxygenated haemoglobin ([HbO_2]), deoxygenated haemoglobin ([HbR]) and total haemoglobin concentration ([HbT], proportional to CBV) (Villringer and Chance 1997). The temporal resolution of NIRS can be better than 10 ms enabling a more accurate characterization of transient phenomena. However, it will be difficult to use NIRS to measure ΔCBF during cerebral activation, as bolus tracking methods must be employed (Kuebler *et al* 1998, Springett *et al* 2001) which are poor for transient measurements. Thus, a NIRS estimate of $\Delta CMRO_2$ requires an assumption to estimate ΔCBF from a measure of ΔCBV, opposite to the requirement of fMRI to estimate ΔCBV from ΔCBF.

Previous visible optical spectroscopy studies have estimated $\Delta CMRO_2$ in animals by thinning or removing the skull to obtain direct visualization of the cerebral vasculature oxygenation and volume, and enable laser Doppler measurements of ΔCBF (Jones *et al* 2001, 2002, Mayhew *et al* 2001b, Zheng *et al* 2002). Using similar model approaches, we investigate whether NIRS can be used to estimate $\Delta CMRO_2$ non-invasively during cerebral activation in humans. We do this with a motor stimulus with rapid presentation of event-like stimuli. We use the Windkessel model (Mandeville *et al* 1999b) to provide a dynamic relationship between ΔCBF and ΔCBV. We explore the various assumptions in the estimate of $\Delta CMRO_2$. While our data predict a most probable $\Delta CBF{:}\Delta CMRO_2$ ratio ranging from 1.5 to 3, in agreement with previous literature findings, we find that better knowledge of the flow–volume relationship, or concurrent measurements of CBF together with NIRS, is required to more accurately quantify the $\Delta CBF{:}\Delta CMRO_2$ ratio. Without this extra knowledge, we find that the NIRS estimate of $\Delta CMRO_2$ cannot significantly distinguish between (1) a tight coupling relationship between $\Delta CMRO_2$ and ΔCBF, and (2) no change in oxygen consumption during activation (i.e. $\Delta CMRO_2 = 0$). The findings presented here highlight the importance of obtaining flow measurements to complement optical results, and demonstrate potential pitfalls in fMRI procedures.

2. Methods

2.1. Instrumentation

The sources in our system are two low-power laser diodes emitting light at discrete wavelengths, 682 nm and 830 nm. A stabilized current, intensity-modulated by an approximately 5 kHz square wave at a 50% duty-cycle, powers these lasers. Both diodes are driven at the same frequency, but phase shifted by 90° with respect to one another. This phase encoding—known as an in-phase/quadrature-phase (IQ) circuit—allows simultaneous laser operation as well as separation of the contributions of each source to a given detector's signal.

The light from each source is directly coupled using standard SMA connectors into a 9 foot long bifurcated glass fibre bundle with a nominal 1 mm core diameter (Fiberoptics Technology, prototype). The light is guided in this source fibre to the scalp of the subject. Detector fibres are also glass fibre bundles, typically with a larger core diameter (2–2.7 mm) but still capable of fitting inside a standard SMA connector.

The system has four separate detector modules (Hamamatsu C5460-01), which are optically and electrically isolated from each other. Each module consists of a silicon avalanche photodiode (APD) with a built-in high-speed current-to-voltage amplifier, and temperature-compensation. They achieve a gain of typically 10^8 V W^{-1} with a noise equivalent power of 0.04 pW $Hz^{-1/2}$ resulting from the high detector sensitivity. The incoming signal at a given detector is composed of both source colours, which are separated by synchronous (lock-in) detection using the two source signals as a reference. The output of the decoding portion of the IQ circuit includes two signal components, corresponding to the two laser wavelengths. The data were sampled at 200 Hz and stored as an ASCII file and then analysed with standard data analysis software packages.

2.2. Motor paradigm

Thirteen healthy subjects were examined (nine female, four male; mean age of 27.1 years, standard deviation 5.1 years). Each subject consented to the experimental procedure, which was approved by the Massachusetts General Hospital internal review board. Subjects laid on their backs on a comfortable pad in a dark and quiet room, with their heads turned slightly to their right so as to be able to see a laptop Macintosh screen. The experiment consisted of three event-related runs. Each run was 10 min in length. The event-related runs consisted of 60 trials, 2 s in duration. Some trials were spaced as little as 2 s apart, while the longest was 33 s apart. Previous research has shown that it is possible to deconvolve trials spaced as close as 2 s (Rosen *et al* 1998). The mean interval between events was 8 s. The sequence of events for each run varied and were generated by a software that produces a sequence of event starting times to optimize the convolution (Dale 1999). Subjects fixated on a laptop screen which presented the words 'STOP' and 'GO' alternately. When they saw GO, they opened and closed their right hands at a rate of approximately 3 Hz for 2 s. They stopped moving when the screen presented the word STOP.

2.3. Optode localization

The light from the lasers was guided to the subjects' heads by optical fibre bundles (optodes). A Velcro headband was fastened snugly around the head to which we attached a flexible piece of plastic cut to hold the optodes firmly in place. Each of four detector fibres that delivered received light back to the photodetectors, was 3.3 cm from the source fibre (see figure 1 for optode positioning on the head relative to the 10-20 system (Jasper 1958)). Since the optodes

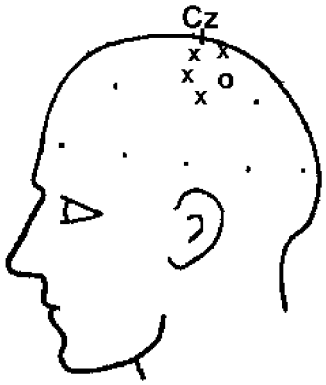

Figure 1. Optode placement for motor paradigm. '0' marks the location of the source, while 'X' marks the location of the detectors.

were all attached to the piece of plastic, their relative positions did not change from subject to subject, though differences in the size of each person's head influenced the precise location of the optodes. It can be reasonably assumed that with this positioning of the optodes that the motor cortex is part of the sampling volume (Homan *et al* 1987, Steinmetz *et al* 1989).

2.4. Data analysis: estimation of haemoglobin concentrations

Subjects were excluded from averaging if their raw data failed to show a plausible heart rate ($n = 4$) or exhibited large motion artefacts ($n = 1$). Eight of the original subjects were retained for further analysis, using three runs of 60 trials each for a grand total of 1440 trials.

The raw 200 Hz data were offset corrected, digitally low-pass filtered at 1 Hz, down sampled to 2 Hz, converted to OD units, and then high-pass filtered with a cut-off frequency of 1/30 Hz to remove any slowly drifting signal components. Finally, each signal pair was converted to relative changes in the concentration of HbR and HbO_2 for each channel using the modified Beer–Lambert Law, the principle of which is described in detail elsewhere (Chance 1991, Cope and Delpy 1988, Villringer and Chance 1997). This equation requires an assumption regarding the differential pathlengths travelled by the two laser light colours. Given the similar total absorption magnitudes for 682 nm and 830 nm light in tissue, we chose our differential pathlength factor (DPF) to be the same for both wavelengths of a given source–detector combination and equal to 6 (Duncan *et al* 1995).

Statistical analysis was performed for individual subjects using the general linear model as outlined by Burock and Dale (2000) and implemented using the FS-FAST analysis package (Burock and Dale 2000). The covariance of noise was not estimated (i.e., white noise was assumed). This approach makes no assumptions about the nature of the haemodynamic response other than the fact that multiple overlapping responses will add linearly. For further analyses, we used the data from the source–detector pair that exhibited the largest haemodynamic response to activation to minimize cross talk in the estimates of ΔHbR and ΔHbO_2 (Strangman *et al* 2003).

2.5. Definition of $CMRO_2$

The cerebral metabolic rate of oxygen (i.e., oxygen consumption) is simply given by the difference of oxygen flowing into and out of a region. If we assume for notational simplicity

that $SaO_2 = 1$, then the relative change in $CMRO_2$ is given by (Mayhew *et al* 2001b)

$$\left(1 + \frac{\Delta \mathrm{CMRO_2}}{\mathrm{CMRO_{2,o}}}\right) = \left(1 + \frac{\Delta \mathrm{CBF}}{\mathrm{CBF_o}}\right)\left(1 + \frac{\Delta [\mathrm{HbR}]_\mathrm{v}}{[\mathrm{HbR}]_\mathrm{v,o}}\right)\left(1 + \frac{\Delta [\mathrm{HbT}]_\mathrm{v}}{[\mathrm{HbT}]_\mathrm{v,o}}\right)^{-1} \tag{1}$$

with the assumption that SaO_2 is a constant, the subscript 'o' indicates the baseline conditions, and $[HbR]_v$ and $[HbT]_v$ indicate the deoxy-haemoglobin and total haemoglobin concentrations in the localized venous compartment, respectively. The $\Delta CMRO_2$, ΔCBF, $\Delta[HbR]$ and $\Delta[HbT]$ are, in general, functions of time. To simplify expressions throughout the manuscript we do not explicitly write their time dependence. The ratio method (Jones *et al* 2001, Mayhew *et al* 2001a, 2001b) can be used to relate the changes in venous compartment haemoglobin concentrations to the haemoglobin concentration changes across all vascular compartments. This gives

$$\left(1 + \frac{\Delta \mathrm{CMRO_2}}{\mathrm{CMRO_{2,o}}}\right) = \left(1 + \frac{\Delta \mathrm{CBF}}{\mathrm{CBF_o}}\right)\left(1 + \gamma_R \frac{\Delta [\mathrm{HbR}]}{[\mathrm{HbR}]_\mathrm{o}}\right)\left(1 + \gamma_T \frac{\Delta [\mathrm{HbT}]}{[\mathrm{HbT}]_\mathrm{o}}\right)^{-1} \tag{2}$$

where the γ factors relate the fractional haemoglobin changes in the venous compartment to those across all vascular compartments

$$\begin{aligned} \gamma_R &= \left(\frac{\Delta [\mathrm{HbR}]_\mathrm{v}}{[\mathrm{HbR}]_\mathrm{v,o}}\right) \Big/ \left(\frac{\Delta [\mathrm{HbR}]}{[\mathrm{HbR}]_\mathrm{o}}\right) \\ \gamma_T &= \left(\frac{\Delta [\mathrm{HbT}]_\mathrm{v}}{[\mathrm{HbT}]_\mathrm{v,o}}\right) \Big/ \left(\frac{\Delta [\mathrm{HbT}]}{[\mathrm{HbT}]_\mathrm{o}}\right). \end{aligned} \tag{3}$$

With NIRS, we measure $\Delta[HbT]$ and $\Delta[HbR]$ but not ΔCBF. The variation of these formulae for non-steady-state conditions has been discussed in Zheng *et al* (2002).

2.6. Relation between CBF and CBV

Grubb *et al* (1974) observed a relationship between cerebral blood flow (CBF) and blood volume (CBV) in primates by inducing variable hypercapnia to obtain different increments in CBF and CBV. They found that a best fit of $CBV = CBF^{0.38}$. This relation has been used recently in modelling the haemodynamic response to cerebral activation (Buxton and Frank 1997, Davis *et al* 1998, Hoge *et al* 1999a, Mandeville *et al* 1999a). However, this relation was measured for global variation in CBF and CBV and its validity for local changes following brain activation has not been established, nor has it been validated for transient phenomena. Those who have explored this relationship during (focal) brain activation have found an exponent ranging from 0.18 to 0.36 (Jones *et al* 2001, 2002, Mandeville *et al* 1999b) depending on the duration of the activation and furthermore have found that a constant exponent does not strictly hold during the transients of the activation, suggesting much greater complexity in the flow–volume relationship than captured by the Grubb relation. For these reasons, we did not use the Grubb relation in our computation of $\Delta CMRO_2$ but instead consider a mechanical model for the flow–volume relationship as described below.

2.7. The Windkessel model for estimating ΔCBF from ΔCBV

The Windkessel model relates ΔCBF to ΔCBV (Mandeville *et al* 1999b). With a few assumptions, we can thus estimate the ΔCBF response to stimulation from the measured ΔHbT. Briefly, the Windkessel model uses conservation of mass to relate the changes in CBV to changes in the flow of blood IN and OUT of the regional arterial, capillary and venous compartments. The model posits that flow into the region is largely determined by vasomotor control of arterioles and that the capillaries and veins passively respond to arterial pressure

changes. A further assumption lumps the capillary and venous compartments together and calls them a Windkessel compartment. Summarizing Mandeville *et al* (1999b), the model is then given by the relationship

(1) between flow (F), pressure (P) and vascular resistance (R), $P(t) = F(t)\,R(t)$;
(2) between Windkessel volume (V_W) and pressure (P_W), $V_W(t) = A\,P_W(t)^{1/\beta}$;
(3) the resistance in the Windkessel compartment (R_W) is related to the volume by $R_W(t)/R_W(0) = (V(0)/V_W(t))^{\alpha}$ and
(4) arterial volume changes are related to the arterial resistance changes.

These equations provide a physical model of vascular response to pressure and resistance changes. The parameter β represents the vascular compliance and $\alpha = 2$ indicates laminar flow within the vessel. The constant $A = V_W(0)/(F(0)R_W(0))^{1/\beta}$ depends on the initial volume and resistance in the Windkessel compartment $V_W(0)$ and $R_W(0)$, and initial flow $F(0)$. The initial volume fraction of arterial blood, Φ_{art}, is assumed to be somewhere between 0 and 20% as discussed below in the subsection on estimating $\Delta CMRO_2$. From these equations, the Windkessel model then arrives at coupled differential equations for flow and volume changes resulting from arterial resistance changes (Mandeville *et al* 1999b).

$$\frac{\partial V_W}{\partial t} = F_{in}(t) - F_{out}(t) = F_{in}(t) - \frac{P_W(t)}{R_W(t)} = F_{in}(t) - \frac{V_W(t)^{\alpha+\beta}}{A^{\beta} R_W(0) V(0)^{\alpha}} \tag{4}$$

$$F_{in}(t) = \frac{P - P_W(t)}{R_A(t)} = \frac{P - V_W(t)^{\beta}/A^{\beta}}{R_A(t)}. \tag{5}$$

We assume a Gaussian model for the temporal response of arterial resistance during cerebral activation, i.e.

$$R_A(t) = R_A(0) - (R_A(0) - R_{A,min}) \exp\left(-\frac{(t - T_{peak})^2}{\sigma_R^2}\right). \tag{6}$$

The solution of these differential equations then provides the required relationship between ΔCBF and ΔCBV. Note that for simplification we normalize the units such that $F_{in}(0) = F_{out}(0) = 1$, $V_W(0) = F_{in}(0)\tau$ where τ is the Windkessel vascular transit time, and $R_A(0) + R_W(0) = 1$.

In the steady state, the Windkessel formulation produces a power law relationship similar to that employed by Grubb,

$$\frac{F_{in}(t)}{F_{in}(0)} = \left(\frac{V_W(t)}{V_W(0)}\right)^{\alpha+\beta} \tag{7}$$

where the Grubb data measured $(\alpha + \beta)^{-1} = 0.38$.

2.8. Procedure for estimating $\Delta CMRO_2$

We first must assume values for $[HbT]_o$, $[HbR]_o$, γ_R and γ_T. Furthermore, the NIRS measure of Δ[HbT] and Δ[HbR] is accurate up to a multiplicative partial volume factor P_V, which we must assume or fit. Fitting for the partial volume factor ultimately leads to a wide range of values for the estimated fractional changes in [HbT], CBV and $CMRO_2$ as we point out in section 3. We assume that haematocrit remains constant during the haemodynamic response to activation and thus $\Delta[HbT]/[HbT]_o = \Delta CBV/CBV_o$, and we also assume laminar flow, i.e. $\alpha = 2$. From the Windkessel model we must estimate values for the arterial resistance $R_A(0)$, $R_{A,min}$, T_{peak} and ${\sigma_R}^2$, in addition to the Windkessel vascular reserve, β, and the Windkessel transit time, τ. All the model parameters are summarized in table 1.

Table 1. The model fitting parameters defined and the corresponding best fit values for each of the three cases considered. The parameters in bold and marked by an * were not varied in the best fit estimates but were allowed to vary within the specified physiological range for the estimate of the flow–consumption distribution indicated in figure 3.

Description	Symbol	Values [HbT] fit	Diffusion limited	Constant $CMRO_2$	Physiological range
Windkessel parameters					
1. Laminar flow	α	$\mathbf{2}^*$			2
2. Windkessel vascular reserve	β	1.6	0.54	0.074	[0.5]
3. Windkessel (vascular) transit time	τ	3.0 s	0.65 s	0.63 s	[1, 6] s
4. Initial arterial resistance	$R_A(0)$	0.79	0.94	0.77	[0.1, 0.8]
5. Minimum arterial resistance	$R_{A,\min}$	0.63	0.91	0.65	
6. Time to maximum resistance change	T_{peak}	5.5 s	5.8 s	5.8 s	
7. Width of temporal resistance change	σ_R	2.9 s	2.7 s	2.8 s	
8. Volume fraction of arterial blood	ϕ_{art}	$\mathbf{0.15}^*$			[0, 0.2]
NIRS parameters					
9. Total haemoglobin baseline concentration	$[\text{HbT}]_o$	$\mathbf{100}^* \mu\mathbf{M}$			[60, 140]
10. Baseline oxygen saturation	SO_2	$\mathbf{0.65}^*$			[0.55, 0.8]
11. Partial volume factor	P_V	0.005	0.0009	0.0064	
$CMRO_2$ parameters					
12. Venous deoxy-haemoglobin ratio	γ_R	$\mathbf{1}^*$			[0.5, 1.5]
13. Venous total haemoglobin ratio	γ_T	$\mathbf{1}^*$			[0.5, 1.5]

As described in section 3, some of these parameters were held fixed while others were optimized in a nonlinear χ^2 fit to the experimentally measured Δ[HbT]. Given the optimal parameters, and the Windkessel estimate of $\Delta CBF/CBF_o$, we then estimated $\Delta CMRO_2/CMRO_{2,o}$ from equation (2). Individual parameters were allowed to vary widely about central values taken from the literature. We assumed laminar blood flow as described in standard physiology texts (Best and Taylor 1990). This assumption only breaks down in humans for vessels larger than 10 mm or complex branching networks of vessels larger than a few mm. The range for the vascular reserve parameter β was chosen so that the steady state flow–volume exponent $(\alpha + \beta)^{-1}$ covered the range of published values of 0.18 to 0.36 (Jones *et al* 2001, 2002, Mandeville *et al* 1999b). The Windkessel (capillary–venous) transit time was allowed to range as high as 6 s, whereas the actual value should be slightly smaller than the full transit time (4–5 s) observed in MRI bolus tracking studies (Calamante *et al* 1999). Arterial resistance in the cortex is generally assumed to be approximately 65% of the total resistance, but we examined a very wide range in this parameter. The arterial blood volume fraction was assumed to be smaller than 20% (Mintun *et al* 1984). PET measures of $CMRO_2$ generally assume a value of 16% for arterial blood volume (Mintun *et al* 1984) while MRI estimates that utilize blood volume measurements with MION have generally ignored the arterial component (Mandeville *et al* 1999b), thus we examined the range from 0 to 20%. The ranges we assume for [HbT] and haemoglobin oxygen saturation (SO_2) come from (Bevilacqua *et al* 1999, Torricelli *et al* 2001). The range of values for γ_R and γ_T were chosen similar to (Jones *et al* 2001, Mayhew *et al* 2001a, 2001b).

We also consider models for $\Delta CMRO_2$ that enable us to predict Δ[HbR] and $\Delta[HbO_2]$ from the experimentally measured Δ[HbT] and the Windkessel estimate of $\Delta CBF/CBF_o$. We consider two extreme cases. The first is known as diffusion-limited oxygen delivery (Buxton and Frank 1997) in which oxygen consumption is limited by the diffusion of oxygen from the capillaries and thus oxygen consumption is tightly coupled to blood flow induced

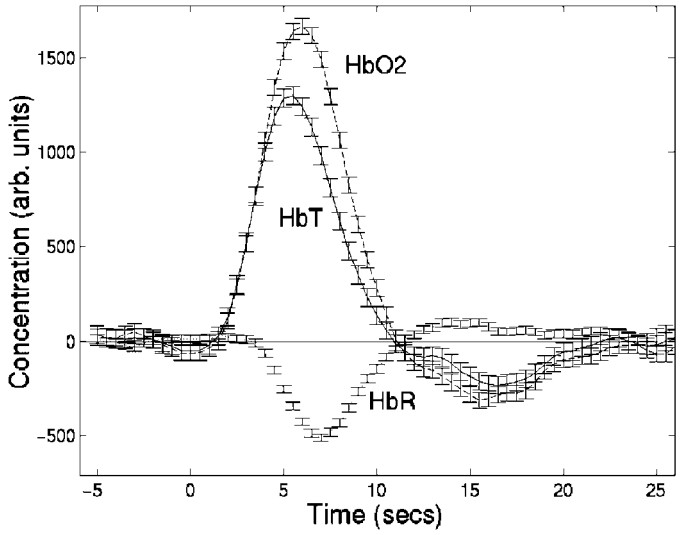

Figure 2. Motor data of the changes in oxy-haemoglobin [HbO_2], deoxy-haemoglobin [HbR] and total haemoglobin [HbT] analysed with differential pathlength factors of 6 and 6 for 682 and 830 nm, respectively. Error bars indicate the standard errors in the estimate from the global average of the eight subjects.

changes in capillary oxygen. Within the diffusion-limited model, we assumed no capillary dilation in order to maintain consistency with the authors' formulation. In the second case we assume that there is no change in $CMRO_2$ during brain activation.

We note that this complex model we are using to fit our experimental data is ignoring some other possible factors, including potential changes in oxygen transport due to capillary dilation (Hyder *et al* 1998), changes in haematocrit during blood flow changes (Pries *et al* 1996) and treating the capillaries separate from the venous compartment within the Windkessel compartment (Mandeville and Rosen 2002). Inclusion of these additional parameters will introduce more flexibility into the model and thus more variability in the estimated flow and $CMRO_2$ changes.

3. Results

3.1. Experimental data

Figure 2 shows the average time courses for Δ[HbR], Δ[HbO_2] and Δ[HbT] from all 1440 trials (or events) of the motor task across the eight subjects. The data show the typical haemodynamic response pattern, with a task-related increase in [HbO_2] and a decrease in the relative concentration of HbR. The response is delayed by approximately 2 s. The onset of the rise in [HbO_2] precedes that of the decrease in [HbR] by $\sim$2 s, and [HbO_2] peaks at $\sim$6 s while [HbR] peaks at $\sim$7 s and [HbT] peaks at $\sim$5 s. There is a post-stimulus overshoot of [HbR] accompanied by a post-stimulus undershoot in [HbT] and [HbO_2], all of which slowly return to baseline. We have minimized the potential for cross talk between NIRS estimates of [HbR] and [HbO_2] changes by using the 682 and 830 nm wavelength pair and analysing the signal from the source–detector pair with the greatest contrast as suggested by Strangman *et al* (Boas *et al* 2001, Strangman *et al* 2003).

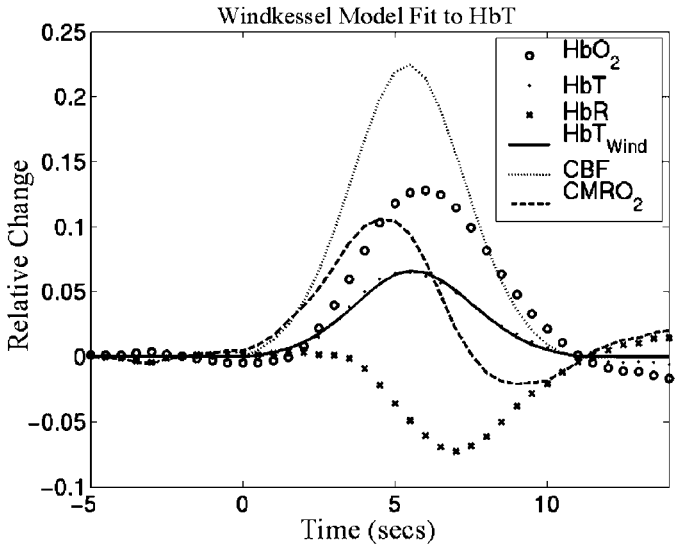

Figure 3. Windkessel model fit to the change in total haemoglobin, HbT and the associated change in CBF. The change in $CMRO_2$ is then calculated from the changes in HbT, CBF and HbR. The ratio of peak change in CBF to peak change in $CMRO_2$ is 2.2.

3.2. Estimation of $\Delta CMRO_2$

To determine $\Delta CMRO_2$ and ΔCBF we first assume $\alpha = 2$, $\Phi_{art} = 0.15$, $[HbT]_o = 100\ \mu M$, $SO_2 = 0.65$, $\gamma_T = 1$ and $\gamma_R = 1$. We then perform a nonlinear fit on the remaining seven parameters indicated in table 1 to obtain an optimal χ^2 fit to the first 12 s of the experimental Δ[HbT] data. The optimal fit has a reduced ${\chi^2}_\upsilon = 1.0$. The fit is shown in figure 3, with the fitted parameter values indicated in table 1. In the fit, we consider only the first 12 s so as to avoid issues with post-stimulus over and undershoots of the haemodynamic parameters. The peak ΔCBF is 22% while the peak $\Delta CMRO_2$ is 10% (a flow–consumption ratio of 2.2).

We can estimate the uncertainty in each model parameter by varying the parameter until the reduced ${\chi^2}_\upsilon$ is increased by 1, while minimizing ${\chi^2}_\upsilon$ by fitting the remaining parameters. Doing so, we find that several of the model parameters are not bounded, while most of the rest have large uncertainties owing to the large number of degrees of freedom (result not shown). This is an intrinsic limitation to estimating $\Delta CMRO_2$ with incomplete haemodynamic information. The wide range of acceptable values for the fitting parameters produces significant variation in ΔCBF and thus $\Delta CMRO_2$. The flow–consumption ratio of the percent changes $\Delta CBF(\%)/\Delta CMRO_2(\%)$, however, has a much reduced variation, particularly when the model parameters are constrained to physiologically relevant values (our chosen physiological range of values is indicated in table 1). The flow–consumption ratio histogram for the range of acceptable model parameters is shown in figure 4 and reveals a most probable ratio of 1.7. This histogram was produced by Monte Carlo sampling of the distribution by selecting random values within the specified range for nine of the parameters and then minimizing ${\chi^2}_\upsilon$ by fitting the remaining four parameters $R_{A,min}$, T_{peak}, σ_R and P_V. The resulting flow–consumption ratio is then weighted by the ${\chi^2}_\upsilon$ value. The distribution was created from 50 000 random samples. We tried two ranges for the arterial blood volume fraction, ranging from 0 to 0.2 and from 0.15 to 0.2, and found only a slight increase in the ratio for the range 0.15 to 0.2.

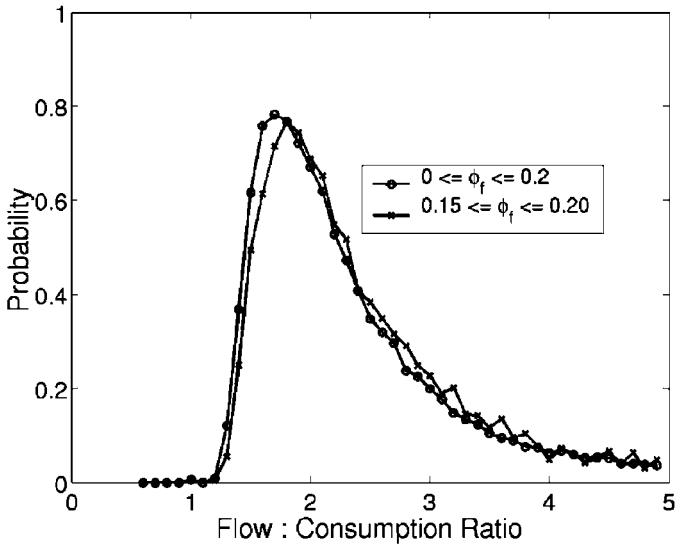

Figure 4. The probability distribution for the estimate of the flow–consumption ratio using the Windkessel model to fit the measured change in total haemoglobin. We considered two ranges for the arterial blood volume fraction.

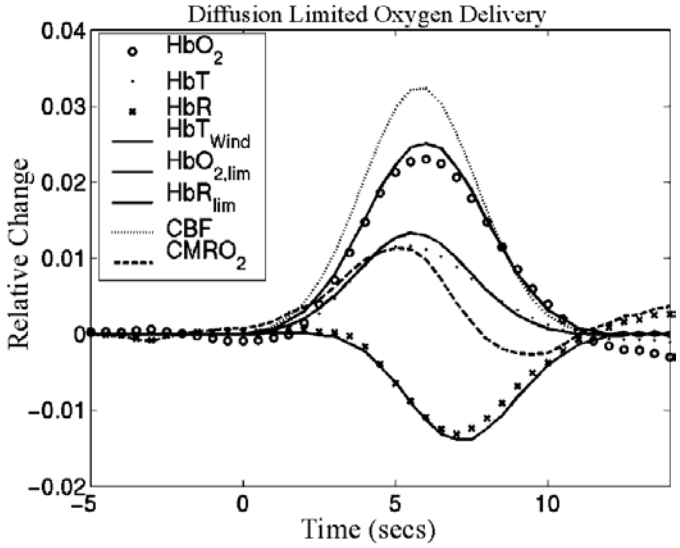

Figure 5. Model fit to total haemoglobin, HbT, oxy-haemoglobin, HbO_2 and deoxy-haemoglobin, HbR, assuming diffusion-limited oxygen delivery.

3.3. Fit assuming diffusion-limited oxygen delivery

First, we assume that changes in oxygen consumption are limited by the diffusion of oxygen from the capillaries, thus providing a direct relationship between $\Delta CMRO_2$ and ΔCBF (Buxton and Frank 1997). A χ^2 fit of [HbO_2], [HbR] and [HbT] assuming the diffusion-limited oxygen delivery model is shown in figure 5. In this fit we first assumed $\alpha = 2$, $\Phi_{art} = 0.15$, $[HbT]_o = 100\ \mu M$, $SO_2 = 0.65$, $\gamma_T = 1$ and $\gamma_R = 1$. We then performed a nonlinear fit

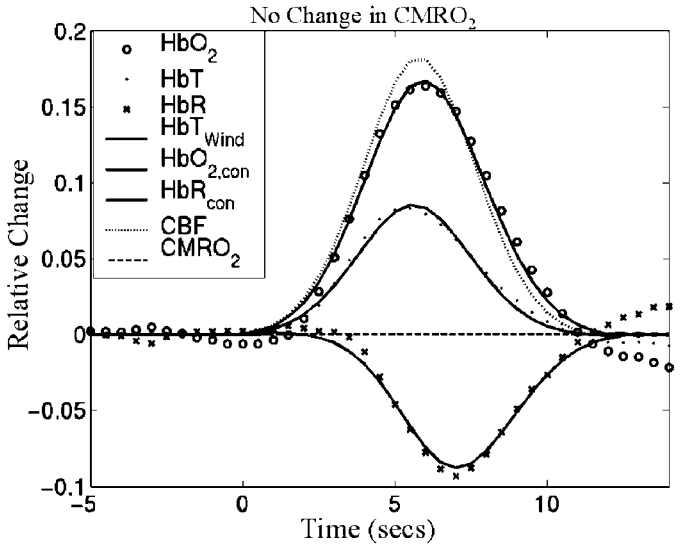

Figure 6. Model fit to total haemoglobin, HbT, oxy-haemoglobin, HbO_2 and deoxy-haemoglobin, HbR, assuming no change in $CMRO_2$.

on the remaining seven parameters indicated in table 1 to obtain an optimal χ^2 fit to the first 12 s of the experimental data. The optimal fit has a reduced ${\chi^2}_\upsilon = 2.4$, and the fitted parameter values are indicated in table 1. The peak ΔCBF is only 3% while the peak $\Delta CMRO_2$ is 1% (a flow–consumption ratio of 3). It is likely that a better reduced ${\chi^2}_\upsilon$ value would be obtained by allowing variation of oxygen diffusivity, haematocrit and arterial resistance changes. Note that the CBV change is only 3% whereas in the previous fit (figure 3), the change was 22%. This significant reduction arises from the fivefold smaller estimate of the partial volume factor (see table 1), which reduces the estimated fractional change in [HbT] and thus also in CBF and $CMRO_2$. Note, however, that the flow–consumption ratio is relatively insensitive to the partial volume factor.

3.4. Fit assuming no change in oxygen consumption

Alternatively, we can assume the extreme case of *no* changes in oxygen consumption in response to cerebral activation. A χ^2 fit of $[HbO_2]$, [HbR] and [HbT] under these conditions is shown in figure 6. In this fit we again assumed $\alpha = 2$, $\Phi_{art} = 0.15$, $[HbT]_o = 100\ \mu M$, $SO_2 = 0.65$, $\gamma_T = 1$ and $\gamma_R = 1$ and performed a nonlinear fit on the remaining seven parameters indicated in table 1 for the first 12 s of the experimental data. The optimal fit also has a reduced ${\chi^2}_\upsilon = 2.4$, and the fitted parameter values are indicated in table 1. The peak ΔCBF is 18% with no change in $\Delta CMRO_2$. Again, it is likely that a better reduced ${\chi^2}_\upsilon$ value would be obtained by allowing variation of oxygen diffusivity, haematocrit and arterial resistance changes.

4. Summary

The estimation of the cerebral metabolic rate of oxygen ($CMRO_2$) requires knowledge of the differential of oxygen flowing into and out of a region of interest. Using the ratio

method (equation (2)), the change in $CMRO_2$ can be determined from the change in blood flow, total haemoglobin concentration and deoxy-haemoglobin concentration. Near-infrared spectroscopy (NIRS) is able to measure relative changes in total haemoglobin and deoxy-haemoglobin concentrations but has not been used to measure flow changes during brain activation. Thus, it is necessary to rely on a model that relates changes in blood flow to changes in blood volume (i.e., total haemoglobin concentration). A commonly employed model (Davis *et al* 1998, Feng *et al* 2003, Hoge *et al* 1999a, 1999b, Kastrup *et al* 1999, Kim and Ugurbil 1995, Kim *et al* 1999, Schwarzbauer and Heinke 1999) is Grubb's relation (Grubb *et al* 1974) which is a power law relation between flow and volume as observed in primates during global haemodynamic modulation by varying fractional inspired CO_2. The validity of this relation during focal brain activation has not been tested extensively, but the few published studies report a wide variation in the exponent (Jones *et al* 2002, Mandeville *et al* 1999b). We therefore utilized a fluid-dynamic model for flow of blood down a series of flexible pipes (i.e., the Windkessel model (Mandeville *et al* 1999b) to fit a flow–volume relationship and model transit time effects, which is essential for describing transient dynamics).

Unfortunately this mechanical model encompasses enough flexibility to produce a wide variation in the flow–volume relationship. We estimated a most probable flow–consumption ratio ranging from 1.5 to 3, within the range of published values which range from 2 to 5.8 (Davis *et al* 1998, Fox *et al* 1988, Hoge *et al* 1999b, Madsen *et al* 1998, Seitz and Roland 1992). However, we also obtained a relatively good fit to the experimental data when we considered the extreme case of no change in oxygen consumption.

Better knowledge of the flow and volume relationship during brain activation (e.g., a tighter constraint on the fitting parameters), or concurrent measurements of flow together with NIRS, is required to obtain a more accurate estimate of the flow–consumption ratio. MRI estimates of $CMRO_2$ using similar methods would appear to be limited by the same problem. However, it has been suggested that when a hypercapnic calibration procedure is utilized, MRI errors in the estimate of $CMRO_2$ are significantly reduced (Davis *et al* 1998). In the absence of this calibration procedure (Kim and Ugurbil 1997), errors should be as unconstrained as in this optical estimation. The utility of a hypercapnic calibration for a NIRS estimate of $CMRO_2$ could be explored. However, further investigation is required to validate an underlying assumption utilized in such a calibration procedure, specifically that the flow–volume relationship is the same for global hypercapnia and localized brain activation; an assumption challenged by recently published data (Zheng *et al* 2002).

Multi-modality imaging provides a potential solution to this quandary. While NIRS can measure changes in blood volume (i.e., total haemoglobin concentration), MRI can measure changes in blood flow (via arterial spin labelling). Thus, through the combination of NIRS and MRI one should be able to obtain an accurate estimate of dynamic changes in $CMRO_2$ during brain activation that does not depend on any model that relates changes in flow to changes in volume. This possibility, together with the assumptions that underpin the hypercapnic calibration procedure employed in MRI, needs further exploration.

Acknowledgments

DAB acknowledges funding from the National Institutes of Health through R29-NS38842, P41-RR14075 and R01-EB00790. JBM acknowledges funding from NIH R01-RR14543. GS acknowledges support via the NIH (P41-RR14075) and the National Space Biomedical Research Institute through NASA Cooperative Agreement NCC 9-58. JPC acknowledges

funding from NIH K25-NS44339. RAP acknowledges support from the Alafi Family Foundation.

References

Best C H and Taylor N B 1990 *Physiological Basis of Medical Practice* (Baltimore, MD: Williams and Wilkins)

Bevilacqua F, Piguet D, Marquet P, Gross J D, Tromberg B J and Depeursinge C 1999 *In vivo* local determination of tissue optical properties: applications to human brain *Appl. Opt.* **38** 4939–50

Boas D A, Gaudette T, Strangman G, Cheng X, Marota J J A and Mandeville J B 2001 The accuracy of near infrared spectroscopy and imaging during focal changes in cerebral hemodynamics *Neuroimage* **13** 76–90

Budinger T F 1998 PET instrumentation: what are the limits? *Semin. Nucl. Med.* **28** 247–67

Burock M A and Dale A M 2000 Estimation and detection of event-related fMRI signals with temporally correlated noise: a statistically efficient and unbiased approach *Hum. Brain. Mapp.* **11** 249–60

Buxton R B and Frank L R 1997 A model for the coupling between cerebral blood flow and oxygen metabolism during neural stimulation *J. Cereb. Blood Flow Metab.* **17** 64–72

Calamante F, Thomas D L, Pell G S, Wiersma J and Turner R 1999 Measuring cerebral blood flow using magnetic resonance imaging techniques *J. Cereb. Blood Flow Metab.* **19** 701–35

Chance B 1991 Optical method *Annu. Rev. Biophys. Biophys. Chem.* **20** 1–28

Cope M and Delpy D T 1988 System for long-term measurement of cerebral blood flow and tissue oxygenation on newborn infants by infra-red transillumination *Med. Biol. Eng. Comput.* **26** 289–94

Dale A M 1999 Optimal experimental design for event-related fMRI *Hum. Brain. Mapp.* **8** 109–14

Davis T L, Kwong K K, Weisskoff R M and Rosen B R 1998 Calibrated functional MRI: mapping the dynamics of oxidative metabolism *Proc. Natl Acad. Sci. USA* **95** 1834–39

Duncan A, Meek J H, Clemence M, Elwell C E, Tyszczuk L, Cope M and Delpy D T 1995 Optical pathlength measurements on adult head, calf and forearm and the head of the newborn infant using phase resolved optical spectroscopy *Phys. Med. Biol.* **40** 295–304

Feng C M, Liu H L, Fox P T and Gao J H 2003 Dynamic changes in the cerebral metabolic rate of o(2) and oxygen extraction ratio in event-related functional MRI *Neuroimage* **18** 257–62

Fox P T, Raichle M E, Mintun M A and Dence C 1988 Nonoxidative glucose consumption during focal physiologic neural activity *Science* **241** 462–4

Grubb R L Jr, Raichle M E, Eichling J O and Ter-Pogossian M M 1974 The effects of changes in $PaCO_2$ on cerebral blood volume, blood flow, and vascular mean transit time *Stroke* **5** 630–9

Hoge R D, Atkinson J, Gill B, Crelier G R, Marrett S and Pike G B 1999a Investigation of BOLD signal dependence on cerebral blood flow and oxygen consumption: the deoxyhemoglobin dilution model *Magn. Reson. Med.* **42** 849–63

Hoge R D, Atkinson J, Gill B, Crelier G R, Marrett S and Pike G B 1999b Linear coupling between cerebral blood flow and oxygen consumption in activated human cortex *Proc. Natl. Acad. Sci. USA* **96** 9403–8

Homan R W, Herman J and Purdy P 1987 Cerebral location of international 10-20 system electrode placement *Electroencephalogr. Clin. Neurophysiol.* **66** 376–82

Hyder F, Shulman R G and Rothman D L 1998 A model for the regulation of cerebral oxygen delivery *J. Appl. Physiol.* **85** 554–64

Jasper H 1958 Report of the committe on methods of clinical examination in electroencephalography *Electroencephalogr. Clin. Neurophysiol.* **10** 370–5

Jones M, Berwick J, Johnston D and Mayhew J 2001 Concurrent optical imaging spectroscopy and laser-Doppler flowmetry: the relationship between blood flow, oxygenation, and volume in rodent barrel cortex *Neuroimage* **13** 1002–15

Jones M, Berwick J and Mayhew J 2002 Changes in blood flow, oxygenation, and volume following extended stimulation of rodent barrel cortex *Neuroimage* **15** 474–87

Kastrup A, Krueger G, Glover G H and Moseley M E 1999 Assessment of cerebral oxidative metabolism with breath holding and fMRI *Magn. Reson. Med.* **42** 608–11

Kim S G 1995 Quantification of relative cerebral blood flow change by flow-sensitive alternating inversion recovery (FAIR) technique: application to functional mapping *Magn. Reson. Med.* **34** 293–301

Kim S G, Rostrup E, Larsson H B, Ogawa S and Paulson O B 1999 Determination of relative $CMRO_2$ from CBF and BOLD changes: significant increase in oxygen consumption rate during visual stimulation *Magn. Reson. Med.* **41** 1152–61

Kim S G and Ugurbil K 1997 Comparison of blood oxygenation and cerebral blood flow effects in fMRI: estimation of relative oxygen consumption change *Magn. Reson. Med.* **38** 59–65

Kohl M, Nolte C, Heekeren H R, Horst S, Scholz U, Obrig H and Villringer A 1998 Determination of the wavelength dependence of the differential pathlength factor from near-infrared pulse signals *Phys. Med. Biol.* **43** 1771–82

Kuebler W M, Sckell A, Habler O, Kleen M, Kuhnle G E H, Welte M, Messmer K and Goetz A E 1998 Noninvasive measurement of regional cerebral blood flow by near-infrared spectroscopy and indocyanine green *J. Cereb. Blood Flow Metab.* **18** 445–56

Madsen P L, Linde R, Hasselbalch S G, Paulson O B and Lassen N A 1998 Activation-induced resetting of cerebral oxygen and glucose uptake in the rat *J. Cereb. Blood Flow Metab.* **18** 742–8

Mandeville J B, Marota J J, Ayata C, Moskowitz M A, Weisskoff R M and Rosen B R 1999a MRI measurement of the temporal evolution of relative CMRO(2) during rat forepaw stimulation *Magn. Reson. Med.* **42** 944–51

Mandeville J B, Marota J J, Ayata C, Zaharchuk G, Moskowitz M A, Rosen B R and Weisskoff R M 1999b Evidence of a cerebrovascular postarteriole windkessel with delayed compliance *J. Cereb. Blood Flow Metab.* **19** 679–89

Mandeville J B, Marota J J A, Kosofsky B E, Keltner J R, Weissleder R, Rosen B R and Weisskoff R M 1998 Dynamic functional imaging of relative cerebral blood volume during rat forepaw stimulation *Magn. Reson. Med.* **39** 615–24

Mandeville J B and Rosen B R 2002 Functional MRI *Brain Mapping: The Methods* ed A W Toga and J C Mazziotta (San Diego: Academic)

Mayhew J, Johnston D, Berwick J, Jones M, Coffey P and Zheng Y 2001a Spectroscopic analysis of neural activity in brain: increased oxygen consumption following activation of barrel cortex *Neuroimage* **13** 540–3

Mayhew J, Johnston D, Martindale J, Jones M, Berwick J and Zheng Y 2001b Increased oxygen consumption following activation of brain: theoretical footnotes using spectroscopic data from barrel cortex *Neuroimage* **13** 975–87

Mintun M A, Raichle M E, Martin W R and Herscovitch P 1984 Brain oxygen utilization measured with O-15 radiotracers and positron emission tomography *J. Nucl. Med.* **25** 177–87

Obrig H, Hirth C, Junge-Hulsing J G, Doge C, Wolf T, Dirnagl U and Villringer A 1996 Cerebral oxygenation changes in response to motor stimulation *J. Appl. Physiol.* **81** 1174–83

Pries A R, Secomb T W and Gaehtgens P 1996 Biophysical aspects of blood flow in the microvasculature *Cardiovasc. Res.* **32** 654–67

Rosen B R, Buckner R L and Dale A M 1998 Event-related functional MRI: past, present, and future *Proc. Natl. Acad. Sci. USA* **95** 773–80

Ross S G, Welch A, Gullberg G T and Huesman R H 1997 An investigation into the effect of input function shape and image acquisition interval on estimates of washin for dynamic cardiac SPECT *Phys. Med. Biol.* **42** 2193–213

Schwarzbauer C and Heinke W 1999 Investigating the dependence of BOLD contrast on oxidative metabolism *Magn. Reson. Med.* **41** 537–43

Seitz R J and Roland P E 1992 Vibratory stimulation increases and decreases the regional cerebral blood flow and oxidative metabolism: a positron emission tomography (PET) study *Acta Neurol. Scand.* **86** 60–7

Springett R, Sakata Y and Delpy D T 2001 Precise measurement of cerebral blood flow in newborn piglets from the bolus passage of indocyanine green *Phys. Med. Biol.* **46** 2209–25

Steinmetz H, Furst G and Meyer B U 1989 Craniocerebral topography within the international 10-20 system *Electroencephalogr. Clin. Neurophysiol.* **72** 499–506

Strangman G, Franceschini M A and Boas D A 2003 Factors affecting the accuracy of near-infrared spectroscopy concentration calculations for focal changes in oxygenation parameters *Neuroimage* **18** 865–79

Torricelli A, Pifferi A, Taroni P, Giambattistelli E and Cubeddu R 2001 *In vivo* optical characterization of human tissues from 610 to 1010 nm by time-resolved reflectance spectroscopy *Phys. Med. Biol.* **46** 2227–37

Villringer A and Chance B 1997 Non-invasive optical spectroscopy and imaging of human brain function *Trends Neurosci.* **20** 435–42

Zheng Y, Martindale J, Johnston D, Jones M, Berwick J and Mayhew J 2002 A model of the hemodynamic response and oxygen delivery to brain *Neuroimage* **16** 617–37